Available online at www.sciencedirect.com

jmr&t Journal of Materials Research and Technology

journal homepage: www.elsevier.com/locate/jmrt

Original Article

Thermal degradation and pyrolysis kinetic behaviour of glass fibre-reinforced thermoplastic resin by TG-FTIR, Py-GC/MS, linear and nonlinear isoconversional models

Samy Yousef [a,c,*], *Justas Eimontas* [b], *Nerijus Striūgas* [b], *Sharath P. Subadra* [a], *Mohammed Ali Abdelnaby* [d]

[a] *Department of Production Engineering, Faculty of Mechanical Engineering and Design, Kaunas University of Technology, LT-51424 Kaunas, Lithuania*

[b] *Lithuanian Energy Institute, Laboratory of Combustion Processes, Breslaujos 3, LT-44403 Kaunas, Lithuania*

[c] *Department of Materials Science, South Ural State University, Lenin Prospect 76, 454080 Chelyabinsk, Russia*

[d] *Department of Production Engineering and Printing Technology, Akhbar Elyom Academy 6th of October, Egypt*

ARTICLE INFO

Article history:
Received 29 June 2021
Accepted 1 November 2021
Available online 8 November 2021

Keywords:
Glass fibre-reinforced polymers
Thermoplastic resin
Pyrolysis treatment
Poly(methyl methacrylate)-PMMA
Pyrolysis kinetics

ABSTRACT

Recently, global demand for glass fibre-reinforced thermoplastic (GFRP) composites and their applications in the production of wind turbine blades has increased due to their bigger strength, impact resistance, toughness, etc. compared to thermosetting resin. In this work, the thermal degradation and pyrolysis kinetic behaviour of GFRP were studied using TG-FTIR, Py-GC/MS, linear and nonlinear isoconversional models to investigate potential applications in the use of pyrolysis technology in end-of-life GFRP treatment. The experiments were carried out on milled glass fibre/poly(methyl methacrylate)-PMMA composites prepared using the vacuum-assisted resin transfer method and the grinding process. The morphological, ultimate, and proximate properties of the feedstock were observed. The thermal and chemical degeneration of the milled GFRP was studied using TG-FTIR, while the composition of the obtained volatile products was identified using Py-GC/MS. With regard to pyrolysis kinetic behaviour of GFRP, the activation energy (Ea) of whole pyrolysis treatment was determined using Kissinger model, while linear and nonlinear isoconversional models were employed to calculate Ea for each conversion phase. Finally, the kinetic methods of distributed activation energy and the independent parallel reactions were employed to fit TG-DTG experimental data. The results revealed that the GFRP is rich in volatile content (49%), while TG-FTIR analysis showed that C–H, C=O, N–O, C–O–C were the main functional groups in the formulated volatile products. Meanwhile, GC/MS measurements showed that methacrylic acid (at 5 °C/min) and 2-Butenoic acid, methyl ester, (Z) (at 10–30 °C/min) were the major compounds in the obtained volatile products with

* Corresponding author.
E-mail address: ahmed.saed@ktu.lt (S. Yousef).

https://doi.org/10.1016/j.jmrt.2021.11.011

abundance of 92% and 88%, respectively. Meanwhile, the kinetic study showed that Ea was estimated at 200 KJ/mol (Kissinger), 143–184 KJ/mol (linear models), and 153–157 KJ/mol (nonlinear model) with R^2 in the range of 92–96.

1. Introduction

Glass fibre-reinforced thermosetting resin (GFRS) and thermoplastic (GFRP) composites are among the most popular lightweight materials [1,2]. These materials are also classified as a key player in case of the structural engineering materials involving them into several applications, such as aircrafts, automotive, marine applications, aerospace, defence industries, energy, wind turbine blades, electronics, etc. [3–5], due to high specific mechanical, chemical, and thermal properties of these materials [6,7]. However, in the recent years, the global demand for GFRP has increased due to their shorter production cycles, higher impact strength and toughness, good recyclability, possibility to be connected easily, stored for long time without any special storage conditions, and ability to be processed more rapidly compared with GFRS [8,9]. Generally, epoxy resin is the most common industrial thermosetting resin product, while poly(methyl methacrylate)-PMMA is a common thermoplastic resin and is used widely in biomaterial applications [10,11], where these different types of thermoplastic resins are used to improve the performance of carbon fibre, glass fibre, natural fibre, etc. using different preparation techniques [12–14].

During the production processes of GFRP composites, a lot of scraps and waste are generated in each production stage along with end-of-life GFRP composites [15,16], what forecasts generation of huge amounts of GFRP waste, hence causing serious health and environmental problems [17]. Therefore, the disposal and valorisation of GFRP waste are becoming a very critical environmental and economic challenge for manufacturers [18]. Usually, landfilling is used to dispose of waste composites without recovery of any added-value products (e.g., energy and raw materials) [19], what causes many negative burdens on the environment in terms of increased amount of greenhouse gases in landfill, contamination of soil and water with toxic gases, and diminished agricultural areas [20]. Based on that, landfilling is considered the worst choice from the economic and environmental point of view. The second choice is incineration that can be used to recover energy in the form of heat [21] with some residues that can be disposed through landfill, too [22]. In order to avoid the limitations of landfill and incineration solutions, many approaches were developed to manage these end-of-life composite and to recycle fully or at least partially the involved raw materials. These processes can be classified into mechanical, thermal and chemical recycling processes [23].

Mechanical recycling consists of two main processes: reduction of the size of GFRS and GFRP by shredding machines followed by the grinding process using hammer mills to produce fine particles. After that, the milled particles can be sorted and separated by sieving, thus, separating resin powder and short fibres combined with resin [24]. The separated resin powder can be processed several times again using common technologies (e.g., hot pressing, extrusion, injection moulding, etc.), and then used for different application [25]. The short fibres combined with resin can be used as filler materials to improve the performance of cement, wood, etc. [26,27]. However, the recovered particles showed several limitations related to compatibility and adhesion with base materials, as well as high viscosity caused by elevated fibre volume fraction, which makes it difficult to process the particles again or decrease their melt viscosity by adding neat resin to powder in order to reach the ideal values [28]. Therefore, Tatariants et al. (2018) used chemical treatment in the dissolution process to purify the extracted short fibre after dissolution of the remining fraction with the help of organic solvents followed by re-extraction of resin from the solution [29,30]. Although the same concept was used to purify fibre, but it was observed that resin degraded and could not be recovered like neat resin, as it had lost some of its properties [31]. Also, this type of treatment needs a big amount of solvents, some of which are classified as toxic and harmful solvents (e.g., DMF, chloroform, etc.), and separation takes longer reaching 72 h [32,33].

What regards thermal practice using pyrolysis, this kind of treatment is used to decompose GFRS and GFRP into lower-weight molecules, including liquid, gases, and solid fractions (char mixed with fibres). Usually, pyrolysis experiments of both GFRS and GFRP are performed using thermogravimetric (TG) for lab scale and a reactor of pilot scale in the range of 450–700 °C (depending on type of resin) [34,35]. The results recommend to perform the treatment at 500 °C to avoid any detrimental impact and degradation of mechanical performance of the recycled fibres [36]. In literature, the majority of the studies were focused on thermal recycling of GFRS, particularly, epoxy resin/glass fibre and studied their pyrolysis kinetics using FTIR and GC/MS [37–39]. However, there is little information on thermal degradation of GFRP and only few studies were performed to understand the pyrolysis behaviour of GFRP. For example, Baek et al. (2018) used pyrolysis treatment to recover carbon fibres from waste PET/carbon fibre composites in the range 400–700 °C [36]. With regard to glass fibre/PMMA, most of the studies were focused on pyrolysis properties of neat PMMA, extruded and cast PMMA, PMMA waste, PMMA–ABS waste, PMMA scraps, PVC/PMMA, CNTs/PMMA using thermogravimetry, pyrolysis reactors and pyrolysis-gas chromatography/mass spectrometry (Py-GC/MS) to recover methacrylic acid and other energy and chemical components [40–47]. In addition, the thermal kinetics of PMMA were studied using different techniques [48–51]. As shown in the literature, the pyrolysis properties of glass/PMMA pyrolysis kinetic parameters are still missing and all this information is necessary for potential upscaling.

In fact, the choosing of a suitable pyrolysis kinetic model is still a matter of debate in the scientific community due to occurring many heterogeneous reactions during the conversion process, what maks hard to propose their pyrolysis kinetics. In this regards, several models have been developed in the literature to study the kinetics of waste pyrolysis in general (like GFRS, which has almost similar composition). These methods can be classified into linear isoconversional models (Kissinger–Akahira–Sunose, Flynn–Wall–Ozawa, and Friedman) and nonlinear isoconversional models (Vyazovkin and Cai). In linear isoconversional models, the activation energies (Ea) at whole conversion zone can be estimated without giving any attention to other kinetics factors, while Ea can be determined using nonlinear isoconversional models through integral mechanical model with high accuracy [52]. Therefore, pyrolysis kinetic behaviour of glass/PMMA were studied in the present research using both models and the distributed activation energy model (DAEM) to calculate both Ea and pre-exponential factor. Also, and in order to encourage the manufacturers to upgrade this technology and invest in it, this research aims to study the basic principle of thermal decomposition of glass/PMMA and its synthesized volatile products using TG-FTIR and GC–MS measurements. In addition, the thermal decomposition curves were modelled using the distributed activation energy model (DAEM) and independent Parallel Reactions Kinetic Model (IPR).

2. Experimental

2.1. Materials and sample preparation

Glass fabric Panda™ (Weave: Twill 2/2 type), Methyl methacrylate (MMA: 617H119-Orthocryl Resin) resin and its polymerizer (Benzoyl peroxide-BPO: Orthocryl resin 617P37, Otto Bock) were purchased from Otto Bock Healthcare GmbH, Waldenbuch, Germany. The samples with 4 layers of Glass fabric with nominal size of 100 mm × 100 mm were prepared according to our previous study. Briefly, at first the resin and polymerizer solution with (PMMA) weight ratio is 100:2 was prepared using a mechanical mixer for 10 min, followed by removal of entrapped air bubbles using a vacuum chamber at 100 bars. Subsequently, glass fibre/PMMA composite panel was fabricated using the vacuum-assisted resin transfer approach followed by curing process using the infrared lamp and industrial oven, respectively [53]. Finally, the prepared cured glass/PMMA panel was milled into fine powder using ball milling (for 20 min and 20 Hz) to minimize mass and heat-transfer resistances during the thermal investigation [54], thus obtaining a uniform glass/PMMA powder ready for the main experiments and analysis.

2.2. Characterization of feedstock

The morphology and microstructure of the fabricated panel and its milled powder were observed using Scanning Electron Microscope (SEM: Model BPI-T) and microscope, respectively. Also, the carbon, nitrogen, hydrogen, sulphur, oxygen content of the powder fraction was determined using PerkinElmer 2400 CHN analyser. In addition, volatile matter, fixed carbon and ash content of the glass/PMMA powder sample were determined on the basis of E1756-01, E872-82, and E1755-01 standards [55,56]. The proximate analysis was carried out using thermogravimetric analysis (TGA) through two stages; a) determination of moisture and volatiles contents and b) determination of fixed carbon and ash contents. In the first stage, the sample was heated till 110 °C under nitrogen with flow rate of 60 mL/min and constant heating rate, then hold the time for 30 min (to achieve an isothermal condition), thus determining the moisture content. After that, the first experiments used a final temperature of 900 °C to identify volatiles content. While the second stage was conducted after switching to an oxidizing ambient in compressed air with flow rate of 100 mL/min, then estimating fixed carbon from the mass loss caused by the chemical reaction between oxygen and fixed carbon at 650 °C (as a starting point). Whereas, the residue fraction represents the ash content of decomposed sample [57]. All measurements were performed three times, then calculating the average. Finally, oxygen content in elemental analysis and fixed carbon content in proximate analysis were determined by differences.

2.3. Thermogravimetric measurements

The thermal decomposition of glass/PMMA powder was investigated using Thermogravimetric analysis (TGA; model: STA449 F3; NETZSCH, Selb, Germany). The experiments were carried out on 7–10 mg of glass/PMMA in a nitrogen ambient with nitrogen flow rate of 60 mL min^{-1}. TGA experiments were conducted at several heating rates to investigate the influence of these heating rates (5, 10, 15, 20, 25, and 30 °C min^{-1}) on the formulated volatile products in the next section. Also, these several heating rates are necessary for studying the pyrolysis kinetic parameters of glass/PMMA and plotting their linear and nonlinear isoconversional curves. The thermal decomposition of glass/PMMA in terms of weight loss was recorded as a function of pyrolysis temperatures using Pyrys software, followed by drawing TGA curves. DTG curves were fitted through numerical derivation of the TGA data, thus estimating the maximum thermal decomposition peak and other pyrolysis parameters of glass/PMMA for all heating rates. Also, the devolatilization index (Di) of volatile matters and the heat-resistance index (THRI) were calculated using Eqs. (1) and (2), respectively [57,58], to check the ability of glass/PMMA to resist a heat flow. They confirm the thermal stability trend obtained from TGA-DTG analysis.

$$D_i = \frac{R_{max}}{(T_i) x\ (T_m)\ x\ (\Delta T)} \quad (1)$$

$$THRI = 0.49 \times [T_5 + 0.6 \times (T_{30} - T_5)] \quad (2)$$

where R_{max}, T_i, T_m, and ΔT in Eq. (1) represent weight loss rate, initial decomposition temperature, maximum decomposition temperature, the changing in temperature in the scope is Rd (decomposition rate)/Rmax = 0.5. T5 and T30 in Eq. (2) represent the corresponding temperature to 5% and 30% of mass losses, respectively. All these parameters can be obtained from TGA-DTG data.

2.4. Chemical analysis of the formulated volatile products

The functional groups of the formulated volatile products at maximum decomposition temperature for each heating rate were examined using thermogravimetrics coupled with Fourier-transform infrared spectroscopy (TG-FTIR). Meanwhile, the composition of the formulated volatile products and their chemical compounds were determined and identified using chromatography–mass spectrometry (GC–MS, Thermo Scientific ISQ™ single quadrupole). The GC–MS measurements were conducted by collecting the resultant gases from decomposition of glass/PMMA in Automation Autoinjector™ connected with TG analyser, then observing it by GC–MS in the scope of 30–600 m/s. The GC–MS analysis was performed under the following column settings: Argon purity ≥99.99%, 20 psi, 100 °C, and 120 s [59,60].

2.5. Pyrolysis kinetics of glass/PMMA

The pyrolysis kinetics of glass/PMMA was started with calculation of activation energy (Ea) of the entire degradation process using Kissinger model, which can be expressed by Eq. (3). In order to determine Ea in each conversion phase in the scope of 10–100%, linear (LIM) and nonlinear isoconversional models (NLIM) were used. Since Kissinger-Akahira-Sunose (KAS), Flynn-Wall-Ozawa (FWO), and Friedman models are the most common LIM methods, therefore, these models were used in the present research to estimate Ea at each conversion rate through the slopes of plotting curves using Eqs (4–6). Regarding NLIM methods, Vyazovkin and Cai are the most common models in this category and can estimate Ea accurately using numerical integration and avoiding the data noises; therefore, Ea for each conversion rate was determined using these models in Eqs (7, 8). Meanwhile, DAEM and IPR models were employed to model TGA-DTG experimental data for each heating rate in Eqs (9, 10). It is worth mentioning that all numerical integrations and algorithms were encoded using MATLAB software. Also, the deviation (Dev.%) between the TGA-DTG experimental and modelled data was checked using Eq. (11). All the above equations are described in Table 1, while the definition of all parameters used in these formulas and their units are illustrated in Table 2.

3. Results and discussion

3.1. Morphology of the prepared glass/PMMA

The morphology of cross-section of the prepared glass/PMMA and its powder batch was checked using SEM and microscope, respectively. Fig. 1A, B shows SEM images of the microstructure cross-section glass/PMMA with scale of 30 and 10 μm. The observation process showed that the panel consisted of several glass laminates containing broken weft and warp yarns (circular shapes). These laminates, including yarns, were collected together using PMMA with regular distribution. Also, some of these yarns were loaded with some PMMA debris in the form of small particles, thus, referring that the fracture was present in glass/PMMA panels because of the brittle failure theory [62]. With regard to glass/PMMA powder batch, the metallurgical image (Fig. 1C) showed that the powder was composed of three fractions on the microscale: short fiberglass, small and black PMMA particles, and short fiberglass coated with PMMA.

3.2. Basic properties of glass/PMMA

Ultimate and proximate measurements of glass/PMMA powder are shown in Table 3. Based on the ultimate measurements, carbon (C) and oxygen (O) are the major elements in the prepared glass/PMMA sample with an average content of 32.15 wt.% and 13.62 wt.%, respectively. In addition to these elements, a small content of hydrogen (H) was noticed at 4.29 wt.%. These elements are classified as a potential source of energy and carbon precursor [63]. As no presence of nitrogen (N) and sulphur (S) was recorded, it means that there were not any toxic emissions (e.g., SO2 and NOx) during the conversion process when the pyrolysis treatment was used at large scale [64,65]. The proximate analysis proves that the glass/PMMA sample is rich in volatile matter (48.88 wt.%), what leads to improvement of the synthesized energy products resulting from the conversion process. Besides, ash component with a high content (49.93 wt.%) was strongly present in the measurements, so, it can be used as a catalyst leading to changed reactivity of glass/PMMA during the conversion process. It may be more activate and improve quality and amount of the obtained liquid fuel [66].

3.3. TG-DTG data analysis

TGA curves of glass/PMMA powder obtained from thermogravimetry for all heating rates are shown in Fig. 2. It is clear that there is only one significant decomposition zone in the temperature range of 280–445 °C with weight loss in the scope of 43 wt.% (25 °C/min)-56 wt.% (5 °C/min) even when the heating rate conditions change. This degradation zone corresponds to full decomposition of PMMA and their organic compounds, including methacrylic acid and its hardener [48]. These results are fully compatible with the preparation conditions of glass/PMMA and PMMA concentration (which was estimated at 38%), what confirms that PMMA component decomposed completely, and fiberglass was mixed with char in the form of solid residues due to higher melting temperature of fiberglass. Also, a very small reduction in weight loss (<1 wt.%) in zone from 25 to 279 °C due to evaporation of moisture was noticed. After 445 °C, char mixed with fiberglass started to formulate until the end of reaction. It is characterised by high thermal stability and is a solid fraction. DTG curves also showed a single reaction peak, what means that all PMMA and hardener's organic components had decomposed together in the form of single reaction [49,50]. Also, it was noticed that the intensity of DTG single peak was increasing as the heating rates increased due to increase in the established heat fluxes, hence facilitating the heat transfer inside the internal molecules of feedstock and decomposition of all their molecules in shorter reaction time [67]. Also, as heating conditions increased from 5 to 30 °C/min, the maximum degradation temperature also increased

Table 1 – Linear and nonlinear isoconversional models used to model the kinetic parameters for pyrolysis of glass/PMMA [55,59,61].

Eq. No.	Method	Expressions	Plots	Slope value
(3)	Kissinger	$\ln\left(\frac{\beta}{T_m^2}\right) = \ln\left(\frac{AR}{E_a}\right) - \frac{E_a}{RT}$	$\ln(\beta/T_m^2)$ versus $1/T$	-Ea/R
(4)	Kissinger-Akahira-Sunose	$\ln\left(\frac{\beta}{T^2}\right) = \ln\left(\frac{AR}{Ea\, g(y)}\right) - \frac{-Ea}{RT}$	$\ln(\beta/T^2)$ versus $1/T$	-Ea/R
(5)	Flynn-Wall-Ozawa	$\ln\beta = \left(\frac{\ln A\, Ea}{R\, g(y)}\right) - 5.335 - \frac{1.0516Ea}{RT}$	$\ln\beta$ versus $1/T$	−1.0516Ea/R
(6)	Friedman	$\ln\left(\beta\frac{dy}{dT}\right) = \ln(Af(y))\left(\frac{-Ea}{RT}\right)$	$\ln(dy/dt)$ versus $1/T$	-Ea/R
(7)	Vyazovkin	$g(y) = \int_0^{\alpha}\frac{dy}{f(y)} = A\int_0^{t}\exp(-E/RT)dt$		-Ea/R
(8)	Cai	$\ln\left\{\frac{\beta_i}{T_{y,i}^2\left[h(x_{y,i}) - \frac{x_{y,i}^2 e^{x_{y,i}}}{x_{y-\Delta y,i}^2 e^{x_{y-\Delta y,i}}}h(x_{y-\Delta y,i})\right]}\right\} = \ln\left\{\frac{A_{y-\Delta y/2}R}{E_{y-\Delta y/2}g(y, y-\Delta y)}\right\} - \frac{E_{y-\Delta y/2}}{RT_{y,i}}$		-Ea/R
(9)	DAEM	$\ln\left(\frac{\beta}{T^2}\right) = \ln\left(\frac{AR}{Ea}\right) + 0.6075 - \frac{Ea}{RT}$		
(10)	IPR	$\frac{dm^{calc}}{dt} = -(m_0 - m)\sum_{i=1}^{3}.C_i\frac{dy_i}{dt}$		
(11)	Dev.%	$\text{Dev.}(\%) = \frac{100\sqrt{\text{F.O.}_{DTG}/N}}{\max(\lvert dm/dt\rvert)}$		

Table 2 – Definition of the parameters of linear and nonlinear isoconversional models.

Parameter	Definition	unit
A	pre-exponential factor	1/min.
T_m	Temperature at maximum reaction rate	°C
β	Heating rate	°C/min.
E_a	apparent activation energy	(J/mol)
R	universal gas constant	(8.314 J/mol K)
g(y)	Integral form of isoconversional function	
T	Absolute Temperature	°C
f(y)	Differential conversion function	
y	Mass loss (Conversion)	
N	Number of experimental data of each run	
m_o	Initial mass	g
m	Mass of the solid	g
Ci	The mass fraction of each of the three subcomponents	
dy/dt	Conversion rate	
x	= Ea/RT	
$h(x)$	The numerically solve function	
$\frac{dm^{calc}}{dt}$	differential weight loss calculated by the model	

progressively from 370 to 399 °C. Finally, the pyrolysis characteristics of glass/PMMA powder in all heating conditions are shown in Table 4. As shown, the thermal stability of glass/PMMA in terms of weight loss changed with changing heating rates.

3.4. FTIR analysis of the formulated compounds

The volatile compounds generated from thermal decomposition of glass/PMMA at the maximum decomposition temperatures in the ranges of 348–399 °C were observed using FTIR coupled with TG. Fig. 3 shows FTIR spectra of the formulated compounds in different heating conditions. The analysis showed that the examined samples had similar functional groups even in changing heating conditions, particularly C–H (aliphatic) group at 2995 cm^{-1}, C=O (aldehyde or ketone) at 1740 cm^{-1}, N–O group at 1457 cm^{-1} and 1250 cm^{-1}, C–O–C (ether) group at 1180 cm^{-1}, and the fingerprint zone in the range of 600–1000 cm^{-1} assigned to C–H bond, which represents the main group in CH2, CH3, and CH gases. It is clear that the absorbances of the groups, especially C–H, C=O, and C–O–C groups, increased significantly as the heating condition increased due to increase in the generated heat flux and all the complex organic molecules decomposed into hydrocarbons compounds [46,48,49]. These results agree with 3D FTIR spectra, which showed a smooth peak separate from other disturbance peaks, especially at higher heating rates. Also, these results manifest that all PMMA organic components have decomposed and converted into chemical compounds with high intensity. The composition of these compounds can be determined using GC/MS measurement, as shown below.

3.5. GC/MS analysis of the formulated volatile products

Fig. 4 and Table 5 show GC/MS results and the composition of the synthesized chemical compounds in their respective peak areas at maximum decomposition temperatures of glass/PMMA samples at 5–30 °C/min. The GC/MS measurements showed that the volatile products obtained from degradation of glass/PMMA using pyrolysis treatment were composed of 2-Propenoic acid, 2-methyl-, methyl ester (Methacrylic acid: 92%) and 2-Propenoic acid, butyl ester (6%) at 5 °C/min. It is worth mentioning that methacrylic acid is used as a precursor to its esters to produce PMMA on industrial scale [44]. Meanwhile, at 10–30 °C/min, 2-Butenoic acid, methyl ester, (Z) ($C_5H_8O_2$) was the major formulated compound with respective peak area in the range from 86 to 88%. This compound has

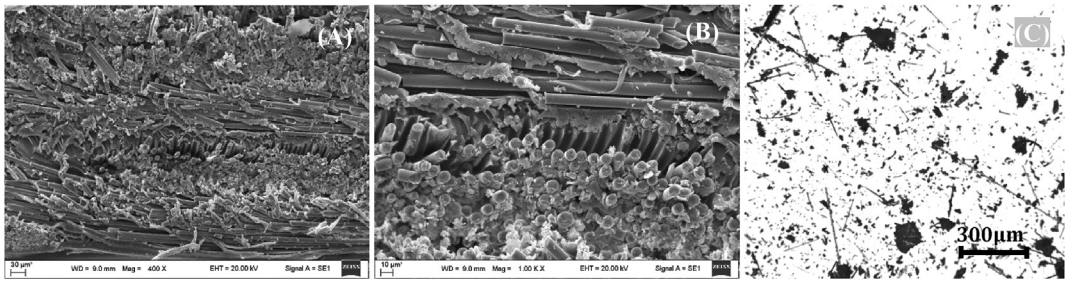

Fig. 1 – A, B) SEM micrograph of the fracture cross-section of glass/PMMA panel, C) Metallographic image of glass/PMMA powder sample.

Table 3 – Ultimate and proximate measurements of glass/PMMA powder.

Elemental analysis (wt. %)					Proximate analysis (wt. %)			
N	C	H	S	O	Moisture	Volatile Matter	Fixed Carbon	Ash
<0.01 ± 0.00	32.15 ± 1.47	4.29 ± 0.19	<0.01 ± 0.00	13.62 ± 0.17	1.09 ± 0.02	48.88 ± 0.28	0.08 ± 0.01	49.93 ± 0.23

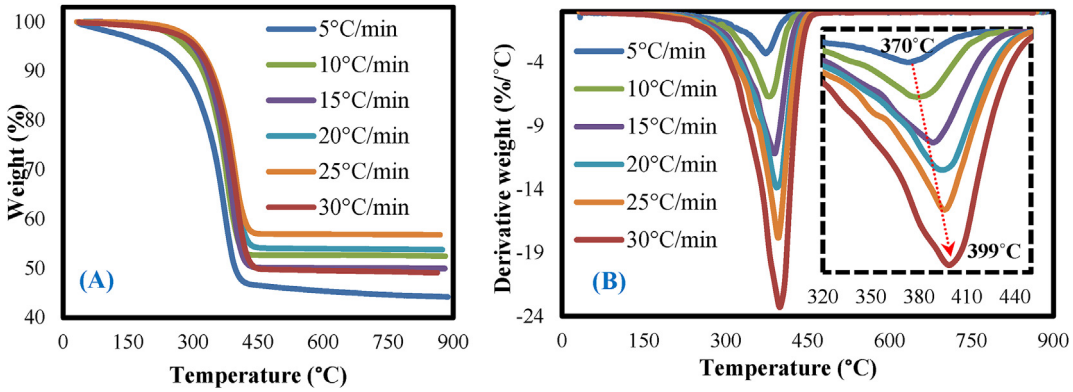

Fig. 2 – A) DTG and B) DTG analysis of glass/PMMA in different heating conditions.

Table 4 – The pyrolysis characteristic of glass/PMMA in different heating conditions.

Pyrolysis parameters	Heating rate (°C/min)					
	5	10	15	20	25	30
Onset temperature Ti (°C)	196	197	200	212	227	245
Tm (°C)	370	374	390	392	397	399
Tf (°C)	437	453	448	474	468	473
Rmax (%/min)	3.3	6.6	11.2	13.2	17.8	23.3
Di (% min−1 °C^{-3})	8.59E-07	1.42E-06	1.94E-06	2.18E-06	3.09E-06	3.18E-06
ΔT	53	63	74	73	64	75
Mf (%)	56	47	50	46	43	51
T5	207.2	282	296.9	308.4	313.2	307.1
T30	357.6	374.4	381.6	392.5	396.6	389.7
THRI	145.75	165.35	170.38	175.84	177.99	174.76

several applications: it may be used in acetylacetone, acetyl propionyl, angelic acid, coffee furanone, etc. [68]. Also, butyl ester (butyl ethanoate) compound was observed at these heating rates with abundance in the range of 8–10%. Butyl ethanoate is used in several applications, such as synthetic fruit flavouring in foods, solvent in nail polish, high-boiling solvent of moderate polarity, etc. [41]. It is clear that the heating rates have a significant impact on the formulated compounds, however their quantity does not change too much. A strong presence of these compounds confirms that pyrolysis process can be used to convert the organic part of GFRP into different high value-added products (depending on

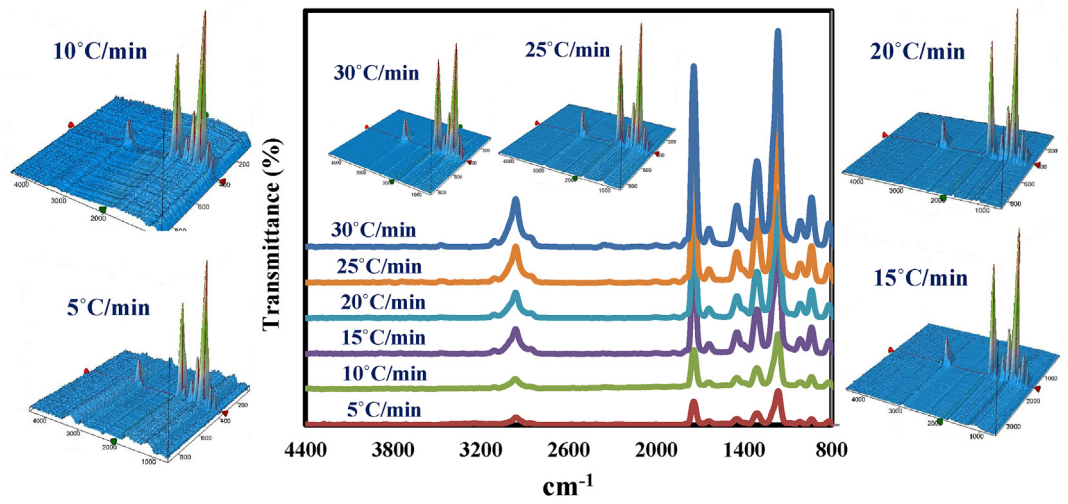

Fig. 3 – 2-3DFTIR analysis of the decomposed glass/PMMA at 5–30 °C/min.

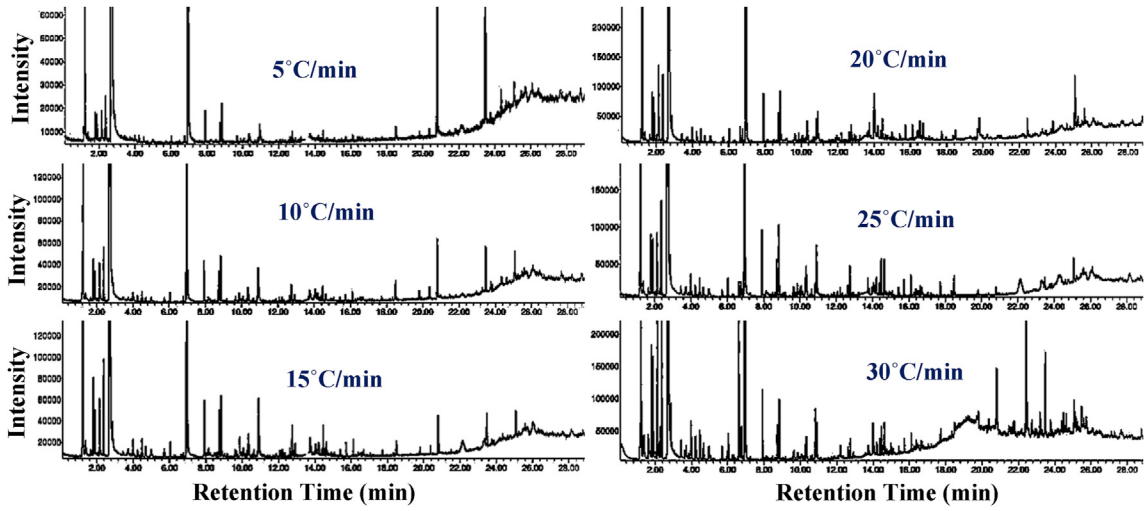

Fig. 4 – GC–MS analysis of the decomposed glass/PMMA at 5–30 °C/min.

the applied heating rates), in addition toshort glass fibres mixed with char fraction.

3.6. *Kinetic analysis of glass/PMMA pyrolysis*

This part was divided into four sections: the first section was focused on calculation of activation energy for the entire pyrolysis process of glass/PMMA using Kissinger model. The second and third sections were used to determine Ea at each conversion rate using linear (KAS, FWO, and Friedman) and nonlinear (Vyazovkin and Cai) isoconversional methods. Meanwhile, the last section was developed to simulate TGA-DTG experimental data using DAEM and IPR models.

3.6.1. *Activation energy for the entire pyrolysis process*

In order to determine the activation energy for the entire pyrolysis process of glass fibre/PMMA using Kissinger model, at first, the relationship between $\ln(\beta/T_m^2)$ versus $1/T$ was plotted in Fig. 5A, then the slope fitted linear curve was estimated, which is represented as $-Ea/R$ ($R = 8.31$ JK^{-1} mol^{-1}). Ea was estimated at 200.48 kJ mol^{-1}. These results are almost similar to Ea determined for PMMA in the reported results in literature, which were estimated at 165–193 kJ/mol (glass/epoxy) and 198, 188.8, 158 kJ/mol (PMMA) [43,48,50], while comparison with Ea of glass fibre/epoxy (165–193 kJ/mol) [39] revealed that glass fibre/PMMA had a little higher Ea. This is due to the fact that glass/PMMA used in the current research was composed of two main components, glass fibre and PMMA, and each component had different Ea. However, glass fibre was not allowed to decompose, while PMMA decomposed in a single reaction (based on the DTG results) and the obtained Ea represents the summation of Ea of all decomposed PMMA components. That is why the pyrolysis of glass/PMMA showed higher Ea compared to other feedstocks. This difference in results is determined by different chemical compositions, sizes, crystallinity, and testing ambient, which led to digestibility of glass/PMMA and its conversion into energy products [43,48,50].

3.6.2. *Estimation of activation energies using isoconversional methods*

The fitted KAS, FWO, and Friedman fitting curves in conversion range of 30–90% are shown Fig. 5B-D. The values of Ea for each conversion rate were calculated using the listed models by determining the slope of these curves. It seems that the curves obtained from all models contained parallel straight lines in the range of 30–90% and this region represented the main conversion zone. However, at 90% conversion rate, straight lines presented a big variation in Friedman model due to fact that this model is very sensitive to data noises [52]. At lower conversion range (10 and 20%), straight lines were observed, but they were fitted and distributed randomly with a big variation. This means that the linear isoconversional method, including KAS, FWO, and Friedman models, is valid to study and model the reaction mechanism of glass/PMMA pyrolysis only in the main conversion zone (30–90%). The calculated Ea and its coefficient of determination (R2) for each model are illustrated in Fig. 6 and Table 6. The results showed that average Ea was estimated at 143.29 kJ mol−1 (KAS), 170.16 kJ mol−1 (FWO), and 184.85 kJ mol−1 (Friedman) with a very small error and R2 was estimated at 0.94 (KAS), 0.96 (FWO), and 0.92 (Friedman). It is clear that Friedman model has the lowest R2 because of its sensitivity to noise data that affect negatively accuracy of the calculated Ea. When these results were compared with the reported results in literature, pyrolysis of glass/PMMA proved Ea almost similar to Glass Fibre-Reinforced Epoxy Resin Composites (165–193 KJ/mol) [39]. Also, for complete thermal decomposition of glass fiber, this fraction needs a very high temperature (>900 °C), what confirms that pyrolysis process can be used to decompose PMMA fraction only [35], thus the calculated Ea represents summation of Ea of all decomposed PMMA resin components. When these results were compared with pyrolysis of PMMA resin only, the values of which were estimated at 213.4 kJ/mol (Friedman),166.7 kJ/mol (KAS), and 218.7 kJ/mol (FWO) [69], it was revealed that the present results showed a little

Table 5 – GC–MS compounds generated at 5–30 °C/min.

0 wt.%			2.5 wt.%			5 wt.%		
Time (min.)	GC Compounds	Area (%)	Time (min.)	GC Compounds	Area (%)	Time (min.)	GC Compounds	Area (%)
1.226	1-Propene, 2-methyl-	0.76	1.232	1-Propene, 2-methyl-	0.93	1.226	1-Butene	2.21
2.688	2-Propenoic acid, 2-methyl-, methyl ester	92.00	2.701	2-Butenoic acid, methyl ester, (Z)	86.97	2.371	Propanoic acid, 2-methyl-, methylester	0.40
6.951	2-Propenoic acid, butyl ester	5.97	6.951	2-Propenoic acid, butyl ester	8.05	2.694	2-Butenoic acid, methyl ester, (Z)	87.30
20.807	2-Propenoic acid, 2-methyl-, 1,2-ethanediylbis(oxy-2,1-ethanediyl) ester	0.58	20.800	2-Propenoic acid, 2-methyl-, 1,2-ethanediylbis(oxy-2,1-ethanediyl) ester	0.30	6.944	2-Propenoic acid, butyl ester	10.09
23.478	1-Propene-1,2,3-tricarboxylic acid, tributyl ester	0.69						

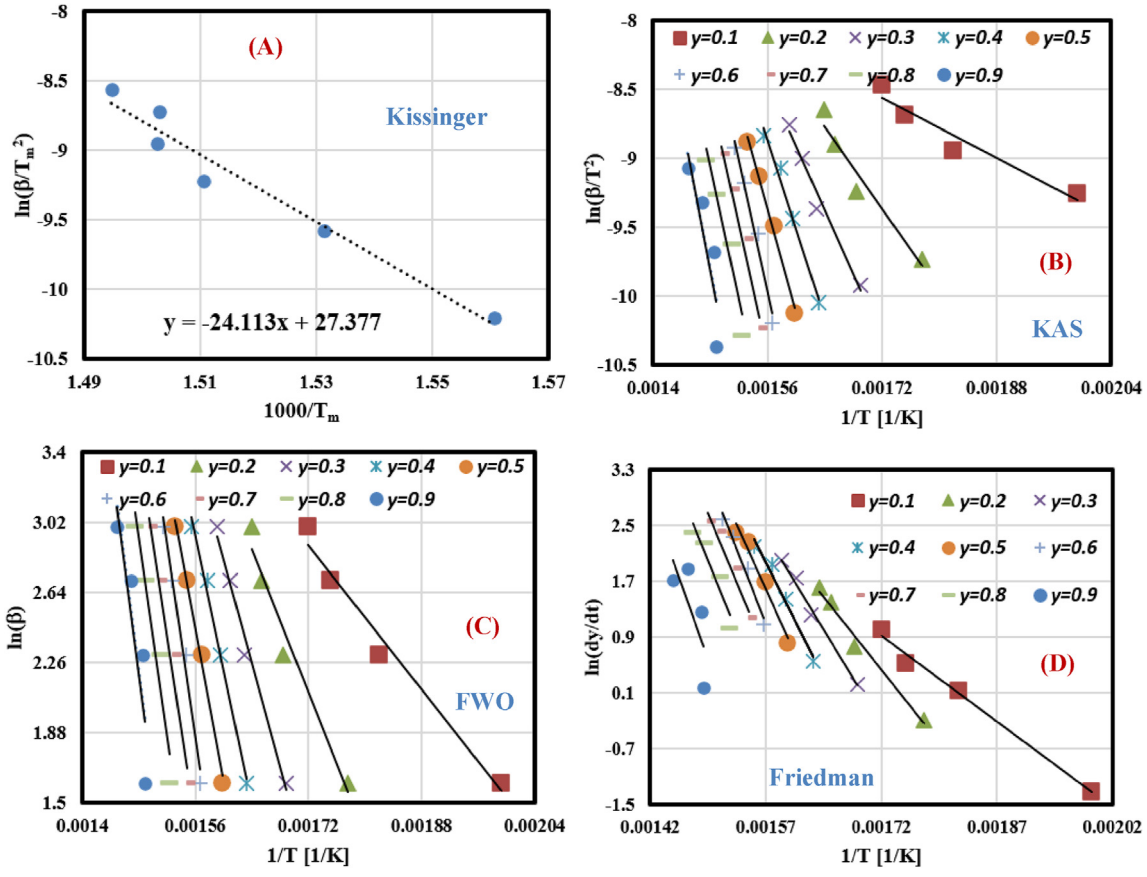

Fig. 5 – Plots of isoconversional methods at different values of conversion.

10 wt.%			20 wt.%			50 wt.%		
Time (min.)	GC Compounds	Area (%)	Time (min.)	GC Compounds	Area (%)	Time (min.)	GC Compounds	Area (%)
1.226	1-Propene, 2-methyl-	1.84	1.226	1-Propene, 2-methyl-	1.44	1.226	1-Propene, 2-methyl-	1.31
2.138	1-Butanol	0.80	2.371	Propanoic acid, 2-methyl-, methylester	0.71	2.138	1-Butanol	0.47
2.371	Propanoic acid, 2-methyl-, methylester	0.75	2.707	2-Butenoic acid, methyl ester, (Z)	88.33	2.364	Propanoic acid, 2-methyl-, methylester	0.40
2.707	2-Butenoic acid, methyl ester, (Z)	85.82	6.944	2-Propenoic acid, butyl ester	9.52	2.714	2-Butenoic acid, methyl ester, (Z)	88.39
6.944	2-Propenoic acid, butyl ester	9.28				6.608	Cyclohexanol	0.41
14.021	p-Isopropenylphenol	1.21				6.938	2-Propenoic acid, butyl ester	7.69
25.069	Piperonal, 6-(4-methoxy-1-cyclohexen-1-yl)-	0.31				20.806	15-Methyl-docosanoic acid, pyrrolidide	0.27
						22.430	4,4'-(Hexafluoroisopropylidene) diphenol	1.06

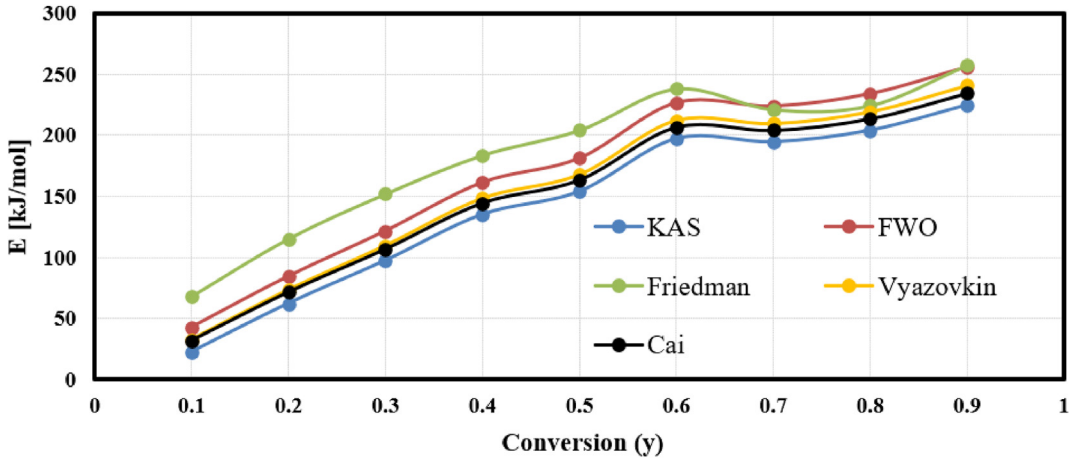

Fig. 6 – Plots of isoconversional methods at different values of conversion.

Table 6 – The estimated activation energy at different conversion rates.

y	KAS (KJ/mol)	R^2	FWO (KJ/mol)	R^2	*Friedman* (KJ/mol)	R^2	*Vyazovkin* (KJ/mol)	R^2	*Cai* (KJ/mol)	R^2
0.1	22.36	0.9313	42.69	0.978	67.91	0.992	32.48	0.9644	31.63	0.9768
0.2	62.07	0.9436	84.46	0.9654	115.16	0.9832	73.34	0.9568	71.41	0.9643
0.3	97.21	0.9775	121.53	0.9839	151.89	0.992	109.55	0.9812	106.67	0.984
0.4	134.86	0.9885	161.24	0.9911	183.66	0.9769	148.33	0.9899	144.43	0.991
0.5	153.66	0.9911	181.09	0.9929	204.10	0.9671	167.72	0.9921	163.30	0.9937
0.6	196.88	0.9773	226.62	0.981	238.03	0.97	212.20	0.9794	206.61	0.9816
0.7	194.26	0.9743	223.82	0.9785	221.15	0.9646	209.53	0.9766	204.02	0.9796
0.8	203.74	0.9243	233.98	0.9358	224.36	0.9211	219.30	0.9306	213.53	0.9376
0.9	224.58	0.7674	256.04	0.795	257.43	0.5387	240.80	0.7824	234.46	0.7979
Avg.	143.29	0.9417	170.16	0.955	184.85	0.9228	157.03	0.9504	152.90	0.956

Table 7 – The determined activation energy using Vyazovkin method at different number of iterations.

Conversion (y)	The Activation Energy (kJ/mol)				
	Initial Value	First Iteration	second Iteration	third iteration	fourth iteration
0.1	200	32.87	32.48	32.48	32.48
0.2	200	73.59	73.10	73.34	73.34
0.3	200	109.71	109.20	109.55	109.55
0.4	200	148.42	147.86	148.33	148.33
0.5	200	167.77	167.19	167.72	167.72
0.6	200	212.19	211.51	212.20	212.20
0.7	200	209.53	208.88	209.53	209.53
0.8	200	219.28	218.63	219.30	219.30
0.9	200	240.76	240.08	240.80	240.80
Average	200	157.12	156.55	157.03	157.03

different Ea because of different composition of the feedstock matrix (PMMA mixed with glass fibre). In order to confirm these results and to improve the accuracy of the estimated Ea, Ea was calculated again using nonlinear isoconversional models, as shown in the next section.

3.6.3. *Estimation of activation energies using nonlinear isoconversional methods*

In this section, Ea at each conversion rate was calculated numerically using Vyazovkin and Cai models. When these models are used, the optimal values of Ea can be obtained after several iterations until the calculated values of Ea become constant. The running codes started with initial condition Ea = 200 kJ/mol; all values of Ea and all its iterations are summarised in Tables 7 and 8. Based on these optimal values, Vyazovkin and Cai curves were fitted for all conversion regions, as shown in Fig. 7. The Y-axis in these fitting curves can be expressed using Eq. (14) (Vyazovkin model) and Eq. (15) (Cai model). Finally, and based on the obtained kinetic results of glass/PMMA pyrolysis KAS and FWO linear isoconversional methods, and Vyazovkin and Cai nonlinear isoconversional methods are highly recommended to study the pyrolysis kinetics of glass/PMMA and to calculate their Ea at each conversion rate with R2>95.

3.6.4. *Fitting of TGA-DTG data using DAEM and IPR*

The DAEM and IPR models using Eqs. (11, 12) were employed in this section to fit TGA-DTG experimental data of decomposition

Table 8 – The calculated activation energy using Cai method at different number of iterations.

Conversion (y)	The Activation Energy (kJ/mol)				
	Initial Value	First Iteration	Second Iteration	Third iteration	Fourth iteration
0.1	200	32.00	31.63	31.63	31.63
0.2	200	71.65	71.18	71.41	71.41
0.3	200	106.83	106.33	106.67	106.67
0.4	200	144.51	143.97	144.43	144.43
0.5	200	163.35	162.79	163.30	163.30
0.6	200	206.60	205.95	206.61	206.61
0.7	200	204.02	203.39	204.02	204.02
0.8	200	213.51	212.88	213.53	213.53
0.9	200	234.42	233.76	234.46	234.46
Average	200	152.99	152.43	152.90	152.90

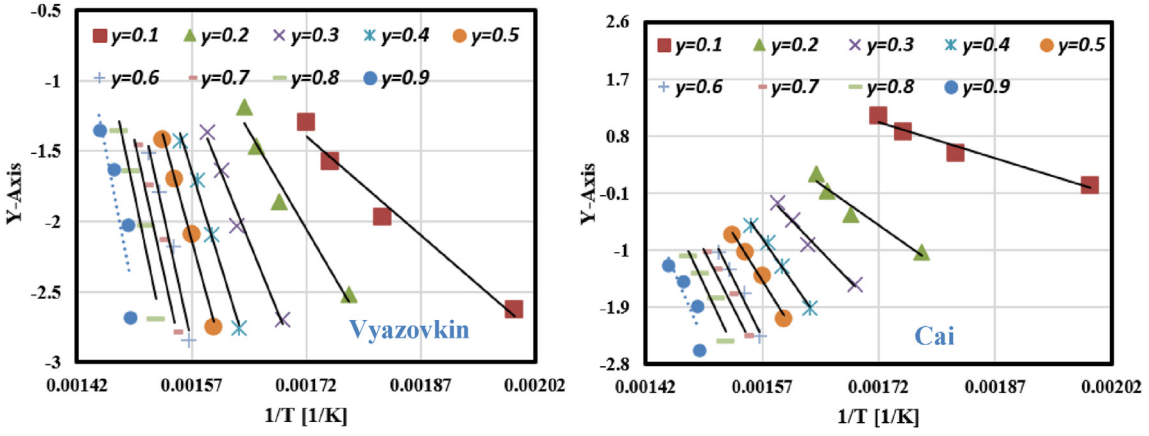

Fig. 7 – Plots of nonlinear isoconversional methods at different values of conversion.

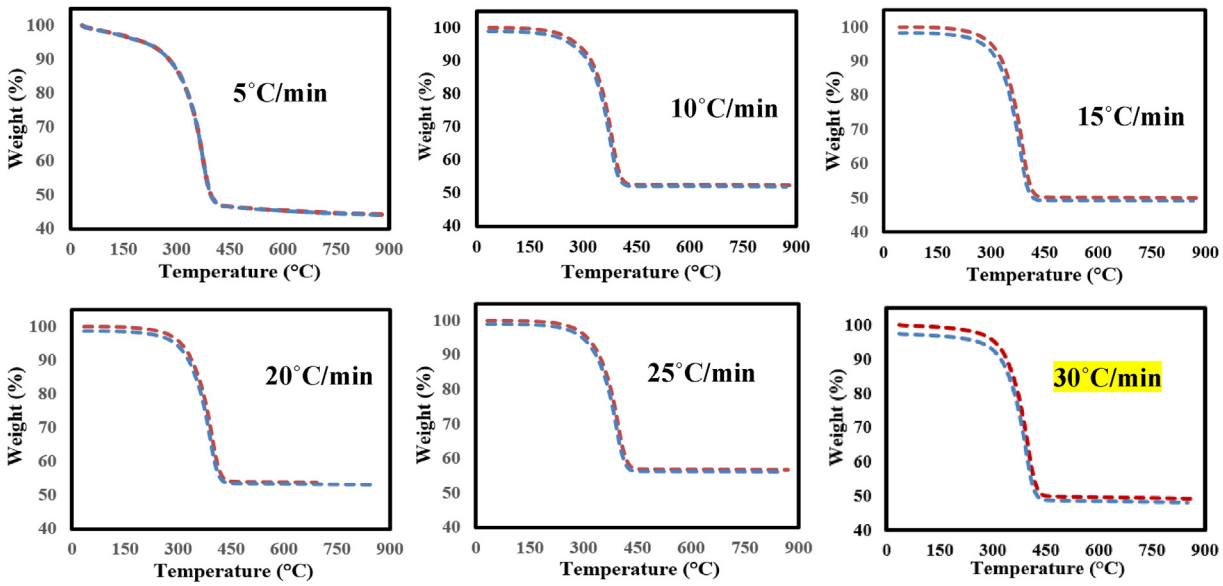

Fig. 8 – TGA experimental and calculated data at 5–30 °C/min.

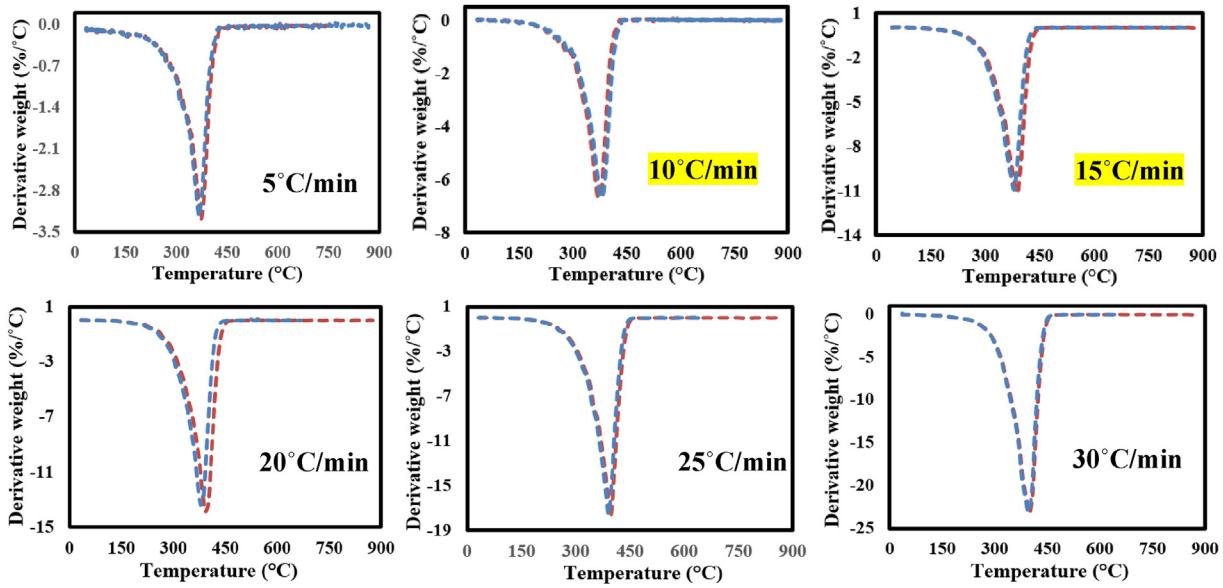

Fig. 9 – DTG experimental and calculated data at 5–30 °C/min.

of glass/PMMA pyrolysis and the fitted curves are shown in (Fig. 8) (TGA curves) and Fig. 9 (DTG curves). In both figures, the experimental data were presented by red dotted lines, while the calculated data were expressed by blue dotted lines. Also, it is clear from both figures that the experimental and calculated curves are match completely with less deviation estimated at 0.8–2.36 for all heating rates in the range of 5–30 °C/min. Based on that, DAEM and IPR models can be used for prediction and fitting of thermal degradation curves of glass/PMMA pyrolysis. Finally, activation energy (E1 and E2) and pre-exponential (A1 and A2) factors were calculated for each model and all values are illustrated in Table 9.

Table 9 – The calculated DAEM and IPR parameters.

	DAEM	IPR
E1	200.382	10.857
A1	3.33E+20	5.55E+14
E2	248.47	234.67
A2	3.66E+20	1.40E+17

4. Conclusions

In this work, the authors studied the fundamental pyrolysis of glass/PMMA using TG-FTIR and GC/MS measurements to

investigate the kinetic by KAS, FWO, Friedman linear isoconversional methods and Vyazovkin and Cai nonlinear isoconversional methods. In order to achieve these goals, the glass/PMMA composite was prepared and its basic properties were observed. Subsequently, the thermal and chemical degradation using TG-FTIR and GC–MS measurements was studied. Finally, the activation energies for each phase were calculated followed by simulating TGA-DTG curves using DAEM and IPR methods. The experiments and analysis of pyrolysis glass/PMMA revealed the following:

a) The thermogravimetric analysis showed that the main pyrolysis stage for glass/PMMA was in the range 196–473 °C with a total mass loss of 43 wt.% at 25 °C/min and 56 wt.% at 5 °C/min. Also, the maximum decomposition temperature was estimated at 370 °C (5 °C/min) and 399 °C (30 °C/min).
b) TG-FTIR analysis showed that C–H, C=O, N–O, C–O–C bonds were the main functional groups in the decomposed glass/PMMA samples and their intensity increased with increase of heating conditions.
c) Py-GC-MS analysis showed that methacrylic acid (92%), 2-Butenoic acid, methyl ester, (Z) (88%) were the major volatile and flammable compounds generated at 5 °C/min and 15–30 °C/min, respectively.
d) The kinetic analysis showed that the average activation energies can be estimated at 200 KJ/mol (Kissinger), 143 KJ/mol (KAS), 170 KJ/mol (FWO), 184 KJ/mol (Friedman), 157 KJ/mol (Vyazovkin), and 153 KJ/mol (Cai) with R^2 in the range 92–96.
e) Meanwhile, DAEM and IPR models showed acceptable results for prediction and modelling of TGA-DTG experimental data of glass/PMMA at different heating rates (5–30 °C/min) with deviation in the range 0.8–2.36.

Based on the obtained results, the pyrolysis treatment has a great potential application in treating a huge amount of glass fibre-reinforced thermoplastic resin waste generated annually without toxic emissions (e.g., SO2 and NOx) during the conversion process and converting PMMA to its original compounds. On the other hand, linear isoconversional, nonlinear isoconversional, DAEM, and IPR models can be used to study the pyrolysis kinetics of glass/PMMA in the main conversion region (30–90%) and to fit TGA-DTG experimental curves with high predictability.

Author statement

Samy Yousef: Conceptualization, Data curation, Formal analysis, Funding acquisition, Investigation, Methodology, Project administration, Resources, Software, Supervision, Writing – original draft, Writing – review & editing.

Justas Eimontas: Conceptualization, Data curation, Formal analysis.

Nerijus Striugas: Conceptualization, Data curation, Formal analysis.

Sharath P. Subadra: Conceptualization, Data curation, Formal analysis.

Mohammed Ali Abdelnaby: Conceptualization, Data curation, Formal analysis, Software, Writing – review & editing.

Declaration of Competing Interest

The authors declare that they have no known competing financial interests or personal relationships that could have appeared to influence the work reported in this paper.

Acknowledgement

This project has received funding from the Research Council of Lithuania (LMTLT), agreement No. S-MIP-20-27.

REFERENCES

[1] Obande W, Ó Brádaigh CM, Ray D. Continuous fibre-reinforced thermoplastic acrylic-matrix composites prepared by liquid resin infusion – a review. Compos B Eng 2021. https://doi.org/10.1016/j.compositesb.2021.108771.
[2] Subadra SP, Griškevičius P, Varnagiris S, Milcius D, Makarevicius V. Superhydrophilic functionalized graphene/fiberglass/epoxy laminates with high mechanical, impact and thermal performance and treated by plasma. Polym Test 2020. https://doi.org/10.1016/j.polymertesting.2020.106701.
[3] Sudhin AU, Remanan M, Ajeesh G, Jayanarayanan K. Comparison of properties of carbon fiber reinforced thermoplastic and thermosetting composites for aerospace applications. In: Materials today: proceedings; 2020. https://doi.org/10.1016/j.matpr.2020.04.297.
[4] Subadra SP, Yousef S, Griskevicius P, Makarevicius V. High-performance fiberglass/epoxy reinforced by functionalized CNTs for vehicle applications with less fuel consumption and greenhouse gas emissions. Polym Test 2020. https://doi.org/10.1016/j.polymertesting.2020.106480.
[5] Tatariants M, Bendikiene R, Kriūkienė R, Denafas G. A new industrial technology for closing the loop of full-size waste motherboards using chemical-ultrasonic-mechanical treatment. Process Saf Environ Protect 2020. https://doi.org/10.1016/j.psep.2020.04.002.
[6] Nash NH, Portela A, Bachour-Sirerol CI, Manolakis I, Comer AJ. Effect of environmental conditioning on the properties of thermosetting- and thermoplastic-matrix composite materials by resin infusion for marine applications. Compos B Eng 2019. https://doi.org/10.1016/j.compositesb.2019.107271.
[7] Kwon DJ, Kim NSR, Jang YJ, Choi HH, Kim K, Kim GH, et al. Impacts of thermoplastics content on mechanical properties of continuous fiber-reinforced thermoplastic composites. Compos B Eng 2021. https://doi.org/10.1016/j.compositesb.2021.108859.
[8] Ke H, Zhao L, Zhang X, Qiao Y, Wang G, Wang X. Performance of high-temperature thermosetting polyimide composites modified with thermoplastic polyimide. Polym Test 2020. https://doi.org/10.1016/j.polymertesting.2020.106746.
[9] Kazemi ME, Shanmugam L, Li Z, Ma R, Yang L, Yang J. Low-velocity impact behaviors of a fully thermoplastic composite laminate fabricated with an innovative acrylic resin. Compos Struct 2020. https://doi.org/10.1016/j.compstruct.2020.112604.
[10] Bîrca A, Gherasim O, Grumezescu V, Grumezescu AM. Introduction in thermoplastic and thermosetting polymers. In: Materials for biomedical engineering: thermoset and thermoplastic polymers; 2019. https://doi.org/10.1016/B978-0-12-816874-5.00001-3.

[11] Pagano S, Lombardo G, Caponi S, Costanzi E, Di Michele A, Bruscoli S, et al. Bio-mechanical characterization of a CAD/CAM PMMA resin for digital removable prostheses. Dent Mater 2021. https://doi.org/10.1016/j.dental.2020.11.003.
[12] Liang EW, Stokes VK. Mechanical properties of injection-molded short-fiber thermoplastic composites. Part 1 : the elastic moduli and strengths of glass-filled poly(butylene terephthalate). Polym Compos 2005. https://doi.org/10.1002/pc.20073.
[13] Kumar V, Yeole PS, Hiremath N, Spencer R, Billah KMM, Vaidya U, et al. Internal arcing and lightning strike damage in short carbon fiber reinforced thermoplastic composites. Compos Sci Technol 2021. https://doi.org/10.1016/j.compscitech.2020.108525.
[14] Awais H, Nawab Y, Amjad A, Anjang A, Md Akil H, Zainol Abidin MS. Environmental benign natural fibre reinforced thermoplastic composites: a review. Composites Part C: Open Access 2021. https://doi.org/10.1016/j.jcomc.2020.100082.
[15] Pegoretti A. Recycling concepts for short-fiber-reinforced and particle-filled thermoplastic composites: a review. Adv Ind Eng Polym Res 2021. https://doi.org/10.1016/j.aiepr.2021.03.004.
[16] Kiss P, Stadlbauer W, Burgstaller C, Stadler H, Fehringer S, Haeuserer F, et al. In-house recycling of carbon- and glass fibre-reinforced thermoplastic composite laminate waste into high-performance sheet materials. Compos Appl Sci Manuf 2020. https://doi.org/10.1016/j.compositesa.2020.106110.
[17] Sarwar Z, Šereika J, Striugas N, Krugly E, Danilovas PP, Martuzevicius D. A new industrial technology for mass production of graphene/peba membranes for CO2/CH4 selectivity with high dispersion, thermal and mechanical performance. Polymers 2020. https://doi.org/10.3390/POLYM12040831.
[18] Amaechi CV, Agbomerie CO, Orok EO, Ye J. Economic aspects of fiber reinforced polymer composite recycling. In: Encyclopedia of renewable and sustainable materials; 2020. https://doi.org/10.1016/b978-0-12-803581-8.10738-6.
[19] Rani M, Choudhary P, Krishnan V, Zafar S. A review on recycling and reuse methods for carbon fiber/glass fiber composites waste from wind turbine blades. Compos B Eng 2021. https://doi.org/10.1016/j.compositesb.2021.108768.
[20] López-García A, Sanz-Aguilar A, Aguirre JI. The trade-offs of foraging at landfills: landfill use enhances hatching success but decrease the juvenile survival of their offspring on white storks (Ciconia ciconia). Sci Total Environ 2021. https://doi.org/10.1016/j.scitotenv.2021.146217.
[21] Keong GC, Mohd Walad MHB, Xiong OW, Haikel MN, Ling CH, Ravichandran RKSO, et al. A study on mechanical properties and leaching behaviour of municipal solid waste (MSW) incineration ash/epoxy composites. In: Energy procedia; 2017. https://doi.org/10.1016/j.egypro.2017.12.780.
[22] Kan L, Shi R, Zhao Y, Duan X, Wu M. Feasibility study on using incineration fly ash from municipal solid waste to develop high ductile alkali-activated composites. J Clean Prod 2020. https://doi.org/10.1016/j.jclepro.2020.120168.
[23] Sommer V, Walther G. Recycling and recovery infrastructures for glass and carbon fiber reinforced plastic waste from wind energy industry: a European case study. Waste Manag 2021. https://doi.org/10.1016/j.wasman.2020.12.021.
[24] Valente M, Sarasini F, Marra F, Tirillò J, Pulci G. Hybrid recycled glass fiber/wood flour thermoplastic composites: manufacturing and mechanical characterization. Compos Appl Sci Manuf 2011. https://doi.org/10.1016/j.compositesa.2011.02.004.
[25] Trofimov E, Eimontas J, Striūgas N, Hamdy M, Abdelnaby MA. Conversion of end-of-life cotton banknotes into liquid fuel using mini-pyrolysis plant. J Clean Prod 2020. https://doi.org/10.1016/j.jclepro.2020.121612.
[26] Clark E, Bleszynski M, Valdez F, Kumosa M. Recycling carbon and glass fiber polymer matrix composite waste into cementitious materials. Resour Conserv Recycl 2020. https://doi.org/10.1016/j.resconrec.2019.104659.
[27] Tomioka M, Ishikawa T, Okuyama K, Tanaka T. Recycling of carbon-fiber-reinforced polypropylene prepreg waste based on pelletization process. J Compos Mater 2017. https://doi.org/10.1177/0021998317694423.
[28] Kalpokaitė-Dičkuvienė R, BaltuŠnikas A, Pitak I, LukoŠiūtė SI. A new strategy for functionalization of char derived from pyrolysis of textile waste and its application as hybrid fillers (CNTs/char and graphene/char) in cement industry. J Clean Prod 2021. https://doi.org/10.1016/j.jclepro.2021.128058.
[29] Tatariants M, Yousef S, Denafas G, Bendikiene R. Separation and purification of metal and fiberglass extracted from waste printed circuit boards using milling and dissolution techniques. Environ Prog Sustain Energy 2018. https://doi.org/10.1002/ep.12899.
[30] Tatariants M, Tichonovas M, Bendikiene R, Denafas G. Recycling of bare waste printed circuit boards as received using an organic solvent technique at a low temperature. J Clean Prod 2018. https://doi.org/10.1016/j.jclepro.2018.03.227.
[31] Oliveux G, Dandy LO, Leeke GA. Current status of recycling of fibre reinforced polymers: review of technologies, reuse and resulting properties. In: Progress in materials science; 2015. https://doi.org/10.1016/j.pmatsci.2015.01.004.
[32] Tatariants M, Yousef S, Denafas G, Tichonovas M, Bendikiene R. Recovery of gold, other metallic and non-metallic components of full-size waste random access memory. J Clean Prod 2018. https://doi.org/10.1016/j.jclepro.2017.11.132.
[33] Cousins DS, Suzuki Y, Murray RE, Samaniuk JR, Stebner AP. Recycling glass fiber thermoplastic composites from wind turbine blades. J Clean Prod 2019. https://doi.org/10.1016/j.jclepro.2018.10.286.
[34] Naqvi SR, Prabhakara HM, Bramer EA, Dierkes W, Akkerman R, Brem G. A critical review on recycling of end-of-life carbon fibre/glass fibre reinforced composites waste using pyrolysis towards a circular economy. Resour Conserv Recycl 2018. https://doi.org/10.1016/j.resconrec.2018.04.013.
[35] Yousef S, Eimontas J, Striūgas N, Abdelnaby MA. Influence of carbon black filler on pyrolysis kinetic behaviour and TG-FTIR-GC–MS analysis of glass fibre reinforced polymer composites. Energy 2021. https://doi.org/10.1016/j.energy.2021.121167.
[36] Baek YM, Shin PS, Kim JH, Park HS, Kwon DJ, DeVries KL, et al. Investigation of interfacial and mechanical properties of various thermally-recycled carbon fibers/recycled PET composites. Fibers Polym 2018. https://doi.org/10.1007/s12221-018-8305-x.
[37] Yun YM, Seo MW, Ra HW, Koo GH, Oh JS, Yoon SJ, et al. Pyrolysis characteristics of glass fiber-reinforced plastic (GFRP) under isothermal conditions. J Anal Appl Pyrol 2015. https://doi.org/10.1016/j.jaap.2015.04.013.
[38] Qiao Y, Das O, Zhao SN, Sun TS, Xu Q, Jiang L. Pyrolysis kinetic study and reaction mechanism of epoxy glass fiber reinforced plastic by thermogravimetric analyzer (Tg) and tg–ftir (fourier-transform infrared) techniques. Polymers 2020. https://doi.org/10.3390/polym12112739.
[39] Eimontas J, Striūgas N, Praspaliauskas M, Abdelnaby MA. Pyrolysis kinetic behaviour of glass fibre-reinforced epoxy resin composites using linear and nonlinear isoconversional methods. Polymers 2021;13:1543. https://doi.org/10.3390/polym13101543.

[40] Özlem-Gundogdu S, Gurel EA, Hacaloglu J. Pyrolysis of of poly(methy methacrylate) copolymers. J Anal Appl Pyrol 2015. https://doi.org/10.1016/j.jaap.2015.03.015.
[41] Braido RS, Borges LEP, Pinto JC. Chemical recycling of crosslinked poly(methyl methacrylate) and characterization of polymers produced with the recycled monomer. J Anal Appl Pyrol 2018. https://doi.org/10.1016/j.jaap.2018.03.017.
[42] Fiola GJ, Chaudhari DM, Stoliarov SI. Comparison of pyrolysis properties of extruded and cast poly(methyl methacrylate). Fire Saf J 2021. https://doi.org/10.1016/j.firesaf.2020.103083.
[43] Ayanoğlu ZG, Doğan M. Characterization and thermal kinetic analysis of PMMA/modified-MWCNT nanocomposites. Diam Relat Mater 2020. https://doi.org/10.1016/j.diamond.2020.107950.
[44] Al-Sagheer F, Ahmad Z. Stabilizing poly(vinyl chloride) using its blends with poly(methyl methacarylate): pyrolysis GC/MS studies. J Hazard Mater 2014. https://doi.org/10.1016/j.jhazmat.2014.06.024.
[45] Szabo E, Olah M, Ronkay F, Miskolczi N, Blazso M. Characterization of the liquid product recovered through pyrolysis of PMMA-ABS waste. J Anal Appl Pyrol 2011. https://doi.org/10.1016/j.jaap.2011.04.008.
[46] Godiya CB, Gabrielli S, Materazzi S, Pianesi MS, Stefanini N, Marcantoni E. Depolymerization of waste poly(methyl methacrylate) scraps and purification of depolymerized products. J Environ Manag 2019. https://doi.org/10.1016/j.jenvman.2018.10.116.
[47] Lopez G, Artetxe M, Amutio M, Elordi G, Aguado R, Olazar M, et al. Recycling poly-(methyl methacrylate) by pyrolysis in a conical spouted bed reactor. Chem Eng Process: Process Intensification 2010. https://doi.org/10.1016/j.cep.2010.08.002.
[48] Korobeinichev OP, Paletsky, Gonchikzhapov MB, Glaznev RK, Gerasimov IE, Naganovsky YK, et al. Kinetics of thermal decomposition of PMMA at different heating rates and in a wide temperature range. Thermochim Acta 2019. https://doi.org/10.1016/j.tca.2018.10.019.
[49] Chen R, Xu M. Kinetic and volatile products study of micron-sized PMMA waste pyrolysis using thermogravimetry and Fourier transform infrared analysis. Waste Manag 2020. https://doi.org/10.1016/j.wasman.2020.05.039.
[50] Jayarama Krishna JV, Srivatsa Kumar S, Korobeinichev OP, Vinu R. Detailed kinetic analysis of slow and fast pyrolysis of poly(methyl methacrylate)-Flame retardant mixtures. Thermochim Acta 2020. https://doi.org/10.1016/j.tca.2020.178545.
[51] Özsin G. Assessing thermal behaviours of cellulose and poly(methyl methacrylate) during co-pyrolysis based on an unified thermoanalytical study. Bioresour Technol 2020. https://doi.org/10.1016/j.biortech.2019.122700.
[52] Yousef S, Eimontas J, Striūgas N, Abdelnaby MA. Pyrolysis kinetic behaviour and TG-FTIR-GC-MS analysis of coronavirus face masks. J Anal Appl Pyrolysis 2021;156:105118. https://doi.org/10.1016/j.jaap.2021.105118.
[53] Subadra SP, Griskevicius P, Yousef S. Low velocity impact and pseudo-ductile behaviour of carbon/glass/epoxy and carbon/glass/PMMA hybrid composite laminates for aircraft application at service temperature. Polym Test 2020. https://doi.org/10.1016/j.polymertesting.2020.106711.
[54] Striūgas Nerijus, Abdelnaby Mohammed Ali. Pyrolysis and gasification kinetic behavior of mango seed shells using TG-FTIR-GC–MS system under N2 and CO2 atmospheres. Renew Energy 2021;173. https://doi.org/10.1016/j.renene.2021.04.034.
[55] Eimontas J, Striūgas N, Mohamed A, Abdelnaby MA. Morphology, compositions, thermal behavior and kinetics of pyrolysis of lint-microfibers generated from clothes dryer. J Anal Appl Pyrol 2021. https://doi.org/10.1016/j.jaap.2021.105037.
[56] Striūgas Nerijus, Eimontas Justas, Abdelnaby Mohammed Ali. Gasification kinetics of char derived from metallised food packaging plastics waste pyrolysis. Energy 2022. https://doi.org/10.1016/j.energy.2021.122070.
[57] Torquato LDM, Crnkovic PM, Ribeiro CA, Crespi MS. New approach for proximate analysis by thermogravimetry using CO2 atmosphere: Validation and application to different biomasses. J Therm Anal Calorim 2017. https://doi.org/10.1007/s10973-016-5882-z.
[58] Eimontas J, Striūgas N, Mohamed A, Ali Abdelnaby M. Pyrolysis kinetic behavior and TG-FTIR-GC–MS analysis of end-life ultrafiltration polymer nanocomposite membranes. Chem Eng J 2022. https://doi.org/10.1016/j.cej.2021.131181.
[59] Eimontas J, Yousef S, Striūgas N, Abdelnaby MA. Catalytic pyrolysis kinetic behaviour and TG-FTIR-GC–MS analysis of waste fishing nets over ZSM-5 zeolite catalyst for caprolactam recovery. Renew Energy 2021. https://doi.org/10.1016/j.renene.2021.07.143.
[60] Eimontas J, Striūgas N, Abdelnaby MA, Yousef S. Catalytic pyrolysis kinetic behavior and TG-FTIR-GC–MS analysis of metallized food packaging plastics with different concentrations of ZSM-5 zeolite catalyst. Polymers 2021. https://doi.org/10.3390/polym13050702.
[61] Striūgas N, Zakarauskas K, Praspaliauskas M, Abdelnaby MA. Pyrolysis kinetic behavior and TG-FTIR-GC–MS analysis of metallised food packaging plastics. Fuel 2020. https://doi.org/10.1016/j.fuel.2020.118737.
[62] Eimontas J, Striugas N, Abdelnaby MA. Modeling of metalized food packaging plastics pyrolysis kinetics using an independent parallel reactions kinetic model. Polymers 2020. https://doi.org/10.3390/polym12081763.
[63] Yang K-T, Hsu J-C, Yang F, Lee S. Mechanical properties of multiwalled-carbon-nanotubes reinforced poly(methyl methacrylate): effect of UV-irradiation. Mater Chem Phys 2021. https://doi.org/10.1016/j.matchemphys.2021.124528.
[64] Šereika J, Tonkonogovas A, Hashem T, Mohamed A. CO2/CH4, CO2/N2 and CO2/H2 selectivity performance of PES membranes under high pressure and temperature for biogas upgrading systems. Environ Technol Innov 2021. https://doi.org/10.1016/j.eti.2020.101339.
[65] Yousef S, Eimontas J, Zakarauskas K, Striūgas N, Mohamed A. A new strategy for using lint-microfibers generated from clothes dryer as a sustainable source of renewable energy. Sci Total Environ 2021. https://doi.org/10.1016/j.scitotenv.2020.143107.
[66] Eimontas J, Zakarauskas K, Striūgas N. Microcrystalline paraffin wax, biogas, carbon particles and aluminum recovery from metallised food packaging plastics using pyrolysis, mechanical and chemical treatments. J Clean Prod 2021. https://doi.org/10.1016/j.jclepro.2021.125878.
[67] Yousef S, Eimontas J, Striūgas N, Tatariants M, Abdelnaby MA, Tuckute S, Kliucininkas L. A sustainable bioenergy conversion strategy for textile waste with self-catalysts using mini-pyrolysis plant. Energy Convers Manag 2019. https://doi.org/10.1016/j.enconman.2019.06.050.
[68] Wang B, Xu F, Zong P, Zhang J, Tian Y, Qiao Y. Effects of heating rate on fast pyrolysis behavior and product distribution of Jerusalem artichoke stalk by using TG-FTIR and Py-GC/MS. Renew Energy 2019. https://doi.org/10.1016/j.renene.2018.08.021.
[69] Bhargava A, Van Hees P, Andersson B. Pyrolysis modeling of PVC and PMMA using a distributed reactivity model. Polym Degrad Stabil 2016. https://doi.org/10.1016/j.polymdegradstab.2016.04.016.